Octupolar Excitation of Ion Motion in a Penning Trap – a Study Performed at LEBIT

R. Ringle [a,b,*] G. Bollen [a,b] P. Schury [a,b] S. Schwarz [a] T. Sun

[a] *National Superconducting Cyclotron Laboratory, East Lansing, MI, USA*

[b] *Department of Physics and Astronomy, Michigan State University, East Lansing, MI, USA*

Abstract

The excitation of the motion of ions in a Penning trap at twice their cyclotron frequency, $2\nu_c$, by means of an azimuthal octupolar RF field has been studied. Presented is the first experimental verification of such an RF octupolar excitation. Compared to ion excitation at ν_c by means of quadrupolar fields an increased resolving power is observed in the cyclotron resonance curves, which may have important implications for Penning trap mass measurements. Numerical simulations have been used to characterize important properties of this type of excitation in detail and to predict the behavior of the ion motion under realistic conditions. Good agreement with the experimental observations is observed. Furthermore, the quadrupolar excitation of the ion motion at ν_c has been revisited and its dependence on the phase of the ion motion and the RF field been studied.

Key words:

PACS: 21.10.Dr, 34.50.Bw, 41.85.Ja, 29.25.Rm

1 Introduction

Penning trap mass spectrometry has proven to be one of the most precise and accurate techniques for the determination of atomic masses of both stable and unstable nuclides. Mass accuracies of 10^{-10} and better have been achieved for stable isotopes, [1–3], providing important data for metrology and QED tests. Mass measurements of unstable isotopes are of interest for nuclear structure studies, for providing key data for fundamental interaction tests, and for a better understanding of the nuclear synthesis of elements in our universe. Despite low production rates and short half-lives mass measurements of short-lived nuclides today reach accuracies of better than 10^{-8} [4,5].

Mass measurements in Penning traps are performed via the determination of the cyclotron frequency $\nu_c = \frac{1}{2\pi}\frac{q}{m}B$ of an ion with mass m and charge q stored in a strong magnetic field. The achievable precision $\delta\nu \propto (\nu \cdot T_{obs} \cdot \sqrt{N})^{-1}$ depends on the frequency ν to be observed, the observation time T_{obs}, and a statistical factor $\sqrt{N}$, where N could be the number of measurements performed or the number of ions detected. In the case of rare isotopes half-lives can be as short as a few milliseconds and beam rates can be well below one ion per second. Since the half-life determines the observation time, gains in precision can only be achieved by maximizing $\nu \cdot \sqrt{N}$. Compared to improving statistics by prolonging the measurement time, if the beam rate is limited, the

* Corresponding author.
Email address: ringle@nscl.msu.edu (R. Ringle).

largest gain factor is obtained by increasing the frequency ν to be observed.

At present, all Penning trap mass spectrometers designed for the study of short-lived nuclides [6–11] employ a technique in which an azimuthal quadrupolar radiofrequency (RF) field is used to excite the radial motion of the ions in the trap [6,12]. At a frequency $\nu_{RF} = \nu_c = \nu_+ + \nu_-$ this field couples the (reduced) cyclotron motion and the magnetron motion, which have eigenfrequencies ν_+ and ν_+. In resonance, a change in energy can be obtained which is detected with a time-of-flight (TOF) resonance detection technique [13].

Several options exist for increasing the frequency ν to be observed. Going towards a higher magnetic field strength is a straightforward approach, realized in the case of LEBIT at the NSCL [7]. More complicated, but with substantial potential, is the employment of highly-charged ions as planned for the TITAN [14] facility at TRIUMF. Another promising idea is to observe higher harmonics in the ion motion in the Penning trap, for example at twice the cyclotron frequency, $2\nu_c$.

General considerations lead one to conclude that an octupolar RF field with a frequency $\nu_{rf} = 2\nu_c$ will drive the ion motion in a resonant manner. One could also expect that the widths of the cyclotron resonances for both quadrupolar and octupolar excitation are in first order fourier-limited and should therefore be the same for a given observation time. In this case the octupolar excitation would yield a factor of two increase in resolving power over the quadrupolar excitation.

The Low Energy Beam and Ion Trap (LEBIT) facility at the NSCL at MSU is the first to perform Penning trap mass measurements on isotopes produced by in-flight separation of relativistic projectile fragments. In order to take

full advantage of this fast production technique, LEBIT has been optimized towards sensitivity and reaching high precision and accuracy for very short-lived nuclides. LEBIT already uses a 9.4 Tesla field, to be compared to 6-7 Tesla used in most of the other systems. LEBIT has been designed to allow for the investigation of octupolar excitation. Early simulations [15] performed at MSU have indicated that octupolar excitation at $2\nu_c$ should indeed be possible and lead to an increase in resolving power.

In this work the first experimental verification of ion motion excitation with an octupolar RF field is presented together with a systematic study of the main features of this new excitation mode. So far no analytical solution has been found for the equations of motion. Therefore, very detailed numerical simulations have been performed to characterize this excitation mode. The simulation results are found to be in excellent agreement with the experimental observations. The most remarkable observation made both in experiment and simulations is a drastic increase in resolving power well beyond the expectation of the factor of two stated above. Similar observations have been made in an independent study [16] at SHIPTRAP at GSI, also presented in this volume. Hence, once fully established, octupolar excitation may provide a significant advance in Penning trap mass spectrometry, in particular for the study of short-lived isotopes.

In the simulation studies of octupolar excitation a strong phase dependence of the ion response was found. This motivated us to revisit the quadrupolar excitation. Both theoretically and experimentally we found that in the case of well-defined phase relations between the RF field and the initial ion motion the resonance shape can become asymmetric. This could provide a possible source of systematic errors in the mass determination if not considered appropriately,

but also a tool for spectrometer diagnostics and tuning.

2 The LEBIT Facility

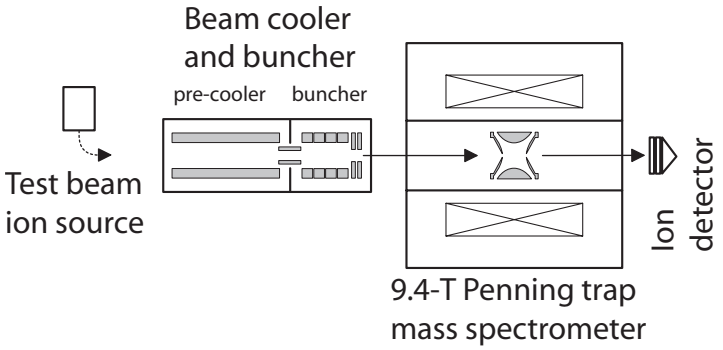

Fig. 1. Partial schematic of the LEBIT facility at the NSCL/MSU. Only components relating to the present work are shown.

The primary experimental goal of the LEBIT, Low Energy Beam and Ion Trap, project is to perform high-precision mass measurements of rare isotopes produced by projectile fragmentation. For this purpose, relativistic rare isotope beams are converted into low-energy beams with excellent quality by using gas stopping and advanced ion guiding, cooling, and bunching techniques [17]. Mass measurements are performed with the LEBIT 9.4 T Penning trap system. In the following a brief summary of the components of the LEBIT facility which are relevant to the present work will be presented.

Fig. 1 shows the components of the LEBIT facility used in the present study. LEBIT is equipped with a plasma ion source station. The plasma ion source provides beams of noble gasses and alkali metals. Most of the measurements presented in this work were performed using $^{23}Na^{+}$ and $^{39,41}K^{+}$. Those ions are transported to the LEBIT beam cooler and buncher [17,18]. The beam cooler and buncher consists of a pair of RFQ ion guide structures which converts

the continuous beam delivered from the ion soucre into a cooled ion pulses which are then delivered to the 9.4 T Penning trap system [7]. The Penning trap system features a high-precision trapping electrode system inside of a room-temperature bore of an actively-shielded 9.4 T persistent superconducting magnet. Holes in the endcaps allow the ions to be injected and ejected by switching the applied potentials to the appropriate endcap electrode. The ring electrode is eight-fold segmented allowing for the application of multipolar RF fields. Dipole RF fields can be used for mass-selective ion removal. Quadrupolar RF fields applied at the proper frequency can be employed to excite the ion's motion at the ion's cyclotron frequency, ν_c [19]. Octupolar RF fields can also be applied, the study of which comprises a majority of this work.

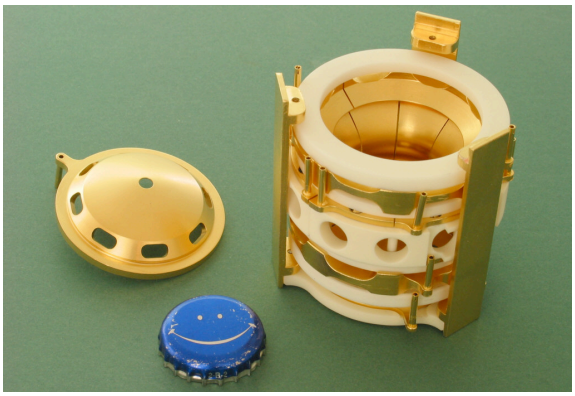

Fig. 2. The LEBIT high-precision Penning trap with the endcap electrode removed. Note the eight-fold segmentation of the hyperbolic ring electrode.

Before the ion pulse from the buncher is captured in the Penning trap an initial magnetron motion is introduced, which is required previous to the application of a quadrupolar RF field. With LEBIT this is accomplished by employing an $\mathbf{E}\times\mathbf{B}$ drift technique using a so-called Lorentz steerer. This steerer is a quartered cylindrical tube at the end of the retardation optics preceding the Penning trap that can be used to create an electric dipole field perpendicular to the magnetic field.

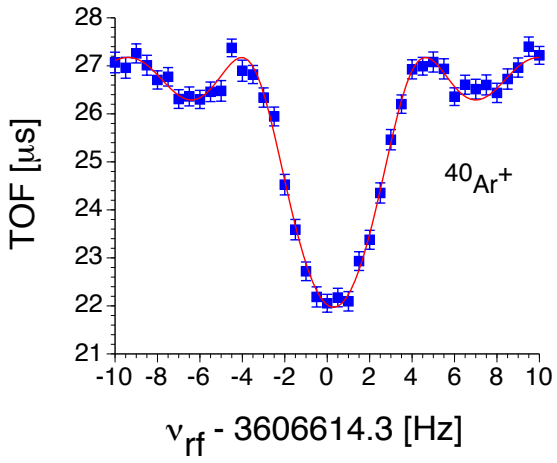

Fig. 3. Quadrupolar resonance curve of $^{40}Ar^{+}$ ions with a fit of the theoretical line shape. An excitation time of T_{rf} = 200 ms was used in this measurement. A full width $\Delta\nu_{FWHM} \approx 4.6$ Hz is observed.

After being captured the ions are exposed to an azimuthal quadrupolar RF field applied at a frequency ν_{rf} close to ν_c. In the case where $\nu_{rf} = \nu_c$, choosing the appropriate RF amplitude and excitation time converts an initial magnetron motion into cyclotron motion, resulting in a gain of radial energy. The energy gain is then detected via a time-of-flight resonance detection technique [12,13,20] in which the ions are ejected from the trap and their time of flight to an ion detector, located outside of the magnetic field, is measured. While passing through the inhomogenous section of the magnetic field the radial energy gained during the excitation is converted into axial energy, reducing the time of flight to the detector. Repeating this process of trapping, excitation, ejection and time of flight measurement for different frequencies results in a resonance curve centered at $\nu_{rf} = \nu_c$. As an example, Fig. 3 shows a sample quadrupolar resonance of $^{40}Ar^{+}$ for an excitation time of T_{rf} = 200 ms. A full width, $\Delta\nu_{FWHM}$, of $\approx 0.9/T_{rf} = 4.5$ Hz is expected [12].

Soon after LEBIT had become fully operational the first octupolar excitation

tests were performed. Fig. 4 shows one of the early resonances, obtained with an excitation of $^{40}Ar^{+}$ also using an excitation time of T_{rf} = 200 ms. A full width of $\Delta\nu_{FWHM} \approx 4.8$ Hz is observed, yielding a factor of two increase in resolving power over an equivalent quadrupolar excitation. However, as is discussed more fully in Chapter 4, simulations and additional measurements show that even greater increases in resolving power should be possible.

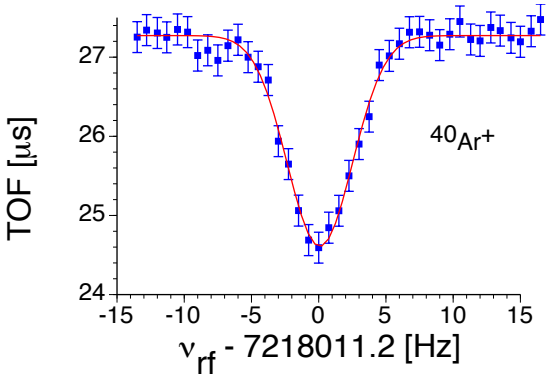

Fig. 4. Octupolar resonance curve of $^{40}Ar^{+}$ with a Gaussian fit. An excitation time of 200 ms was used in this measurement. A full width $\Delta\nu_{FWHM} \approx 4.8$ Hz is observed.

3 Aspects of the Quadrupolar Excitation

In order to provide some background for the discussion of both quadrupolar and octupolar excitations we will briefly review the major steps leading to the equations of motion for a quadrupolar excitation, as derived in [12].

3.1 Equations of motion

Begin by introducing the vectors $\overrightarrow{V}^{+}$ and $\overrightarrow{V}^{-}$ [21] such that

$$\overrightarrow{V}^{\pm} = \dot{\overrightarrow{\rho}} - \omega_{\mp} \cdot \overrightarrow{\rho} \times \hat{e}_z, \tag{1}$$

where $\overrightarrow{\rho}$ is the ion's position vector. Additionally,

$$\begin{aligned} x &= -\tfrac{V_y^+ - V_y^-}{\omega_+ - \omega_-} \\ y &= \tfrac{V_x^+ - V_x^-}{\omega_+ - \omega_-}, \end{aligned} \tag{2}$$

where x and y are the ion's position in Cartesian coordinates. Eq. 1 successfully decouples the equations of motion of an ion confined in a Penning trap. Using this coordinate transformation and applying the rotating wave approximation the equations of motion can be solved [12] for an ion subjected to an applied quadrupolar RF field. The solution is

$$\begin{aligned} \rho_\pm(t) = [&\rho_{\pm,o}\cos(\omega_B t) \mp \\ &\tfrac{1}{2}\tfrac{\rho_{\pm,o}[i(\omega_{rf}-\omega_c)]+\rho_{\mp,o}k_o^\pm}{\omega_B} \\ &\times \sin(\omega_B t)]e^{\frac{i}{2}(\omega_{rf}-\omega_c)t} \end{aligned} \tag{3}$$

where $\rho_\pm$(t) are the magnitudes of the cyclotron and magnetron radii as a function of time and $\rho_{\pm,o}$ are the initial cyclotron and magnetron radii. Additionally,

$$\omega_B = \frac{1}{2}\sqrt{(\omega_{rf}-\omega_c)^2 + k_o^2} \tag{4}$$

and $\mathrm{k}_o^\pm = \mathrm{k}_o \mathrm{e}^{\pm i\Delta\phi}$ where $\mathrm{k}_o = \frac{U_{rf}}{2a^2}\frac{q}{m}\frac{1}{\omega_+ - \omega_-}$. Here, q is the ionic charge, m is the ionic mass, U_{rf} is the applied RF amplitude, a is the radius at which the RF is applied and

$$\Delta\phi = \phi_{rf} - (\phi_+ + \phi_-). \tag{5}$$

ϕ_{rf} is the phase of the applied RF and $\phi_{\pm}$ are the cyclotron and magnetron phases. As stated above, radial energy gained during the excitation process is detected via a reduced time of flight of ions ejected from the trap to the detector. Under normal conditions $\omega_+ \gg \omega_-$, so we can write the radial energy as $\mathrm{E}_r(\mathrm{t}) \approx \frac{1}{2}\mathrm{m}\omega_+^2\rho_+^2(\mathrm{t})$.

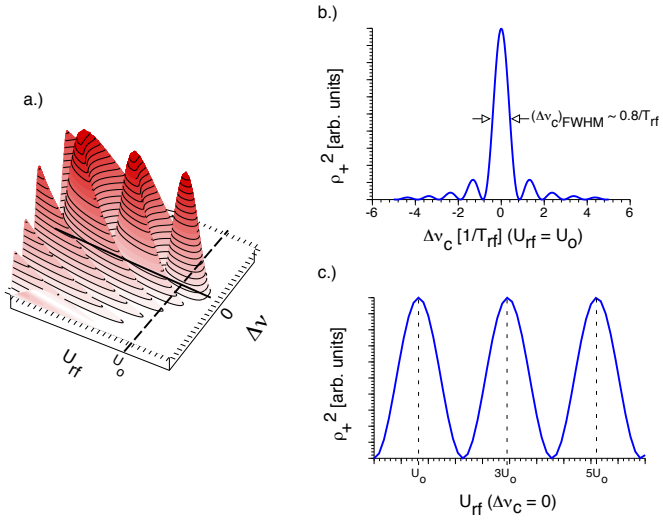

Fig. 5. (a) surface plot of ρ_+^2 as a function of U_{rf} and ν_{rf} for a given excitation time T_{rf}. (b) cut from plot (a) at $\mathrm{U}_{rf} = \mathrm{U}_o$. Full conversion from magnetron to cyclotron motion is achieved at $\Delta\nu_c = \nu_{rf}$ - $\nu_c = 0$. (c) slice from plot (a) at $\Delta\nu = 0$ illustrating the beating of ρ_+^2 as a function of U_{rf}.

Fig. 5(a) shows a calculated 3D plot of ρ_+^2, which is proportional to the gained energy, as a function of U_{rf} and frequency detuning for a given T_{rf} for a single ion initially executing pure magnetron motion, $\rho_{+,o} = 0$. Fig. 5(b) shows a cut at $\mathrm{U}_{rf} = \mathrm{U}_o$, which is the excitation amplitude at which a full conversion of magnetron to cyclotron motion has occurred for $\nu_{rf} = \nu_c$. Such a response is reflected in the experimental resonance curve shown in Fig. 3. Fig. 5(c) is a cut along $\Delta\nu = \nu_{rf}$ - $\nu_c = 0$ illustrating the change of ρ_+^2 as a function of U_{rf} for a constant excitation time.

When performing a quadrupolar excitation for a mass measurement one picks the appropriate combination of amplitude and excitation time, U_{rf} and T_{rf}, such that the initial magnetron motion is fully converted into cyclotron motion, maximizing the radial energy gain of the trapped ions. The resulting line shape at this point has a full width, $\Delta\nu_{FWHM}$, $\sim 0.8/T_{rf}$. Calculating the energy gain from the excitation and accounting for the ejection optics and magnetic field it is possible to calculate the theoretical line shape [12] to be observed in the time-of-flight measurement. This shape has been used to fit the experimental data shown in Fig. 3. Due to a nonlinear conversion between radial energy and time of flight, the full width of the time of flight curve is $0.9/T_{rf}$ for LEBIT.

3.2 Phase dependence of the quadrupolar excitation

The solution to the equations of motion as derived in [12] contains a phase dependence, the consequence of which has not been previously investigated. The phase-dependent term appears in Eq. 3 through the $k_o^{\pm}$ term. We algebraically expand

$$\begin{aligned}\rho_+(t)\rho_+(t)^* = & \frac{4\rho_{+,o}^2\omega_B^2\cos^2(\omega_B t)}{4\omega_B^2} \\ & + \frac{k_o^2\rho_{-,o}^2+\rho_{+,o}^2(\omega_{rf}-\omega_c)^2}{4\omega_B^2}\sin^2(\omega_B t) \\ & - \frac{k_o\rho_{-,o}\rho_{+,o}(\omega_{rf}-\omega_c)\sin(\Delta\phi)}{4\omega_B^2}\sin^2(\omega_B t) \\ & - \frac{2k_o\rho_{-,o}\rho_{+,o}\omega_B\cos(\Delta\phi)}{4\omega_B^2}\sin(2\omega_B t).\end{aligned} \tag{6}$$

The phase dependence of the radial energy change is located in the third and fourth terms of Eq. 6. Both terms scale with the product of $\rho_{+,o}$ and $\rho_{-,o}$, which

means if the ions begin in a state of pure cyclotron or magnetron motion at the beginning of the excitation the effect will not be present.

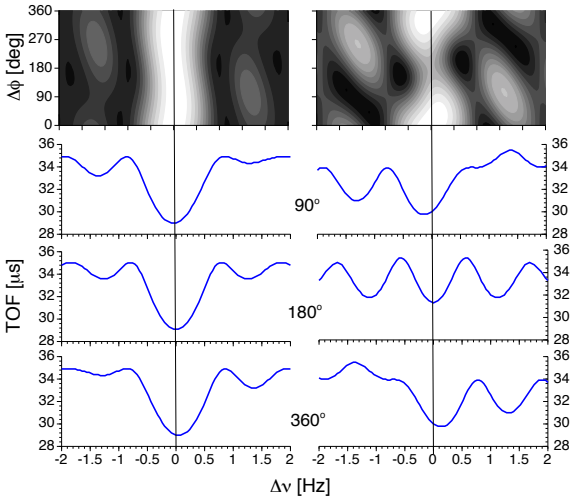

Fig. 6. Simulations of quadrupolar resonances for single $^{39}K^{+}$ ions with $T_{rf} = 1$ s. The two plots in the top row are contour plots of the resonances as a function of $\Delta\phi$ and $\Delta\nu$. Below are cuts at given values of $\Delta\phi$. Both simulations were performed with $\rho_{-,o} = 1$ mm and $\phi_{-,o} = \phi_{-,o} = 0°$. An initial cyclotron radius of $\rho_{+,o} = 0.1$ mm was used on the left and $\rho_{+,o} = 0.4$ mm was used on the right.

Fig. 6 presents the results of simulations of quadrupolar resonances for single $^{39}K^{+}$ ions with $T_{rf} = 1$ s. Both simulations were performed with $\rho_{-,o} = 1$ mm and $\phi_{+,o} = \phi_{-,o} = 0°$. An initial cyclotron radius of $\rho_{+,o} = 0.1$ mm was used on the left and $\rho_{+,o} = 0.4$ mm was used on the right. In each case the value of U_{rf} was adjusted such that in resonance and for $\phi_{rf} = 0°$ the radial energy was maximized. Looking closely at the contour plot on the left one can see a distortion of the central peak and a shift in the position of the side bands as $\Delta\phi$ changes. Resonance profiles for which $\Delta\phi = 90°$ and $180°$ become asymmetric and the position of the minimum time of flight has shifted slightly. Increasing the value of $\rho_{+,o}$ to 0.4 mm only exacerbates the situation. The most obvious implication of these phase-dependent effects involve

low-statistics measurements where $\Delta\phi$ is allowed to vary. If the measurement samples any particular phase range more frequently and the resonance is fit with a line shape with a symmetric center then the analysis will include an additional error.

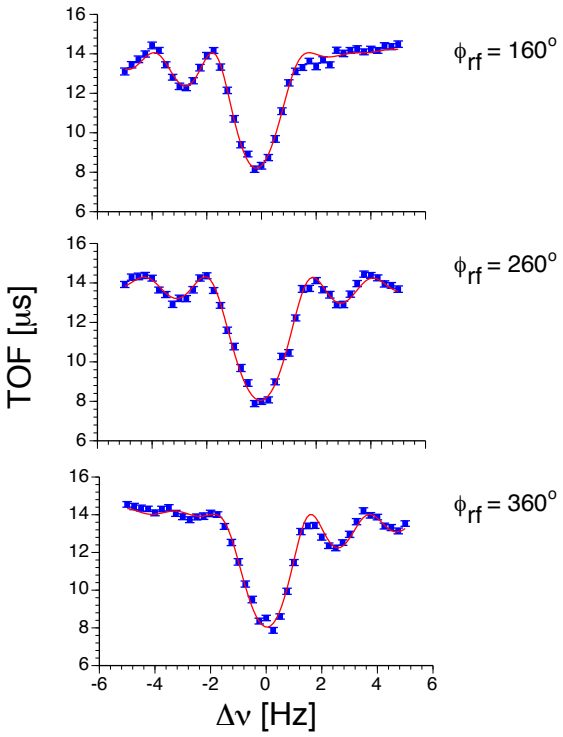

Fig. 7. Three $^{39}K^{+}$ quadrupolar resonances for $T_{rf} = 500$ ms measured for different values of ϕ_{rf}. The solid line is the fit of the theoretical line shape.

In order to see the phase dependence in the radial energy change of the quadrupolar excitation, two conditions must be met. The first is that the RF voltage must have a defined phase relation to initial ion motion. $\Delta\phi$ must not be random which means, according to Eq. 5, that all individual phases must be well defined. If this is not the case then the final line shape will be an average over the line shapes of random $\Delta\phi$'s. The second condition is that the ion ensemble cannot begin in a pure state of cyclotron or magnetron motion.

For the test of this phase dependence $^{39}K^{+}$ ions were injected into the Penning trap, and an initial magnetron motion was introduced with the Lorentz steerer. The excitation RF was phase locked to the time of ion capture in the trap, which defines the initial phase of the ion motion. Several resonances with T_{rf} = 500 ms were taken with varied values of ϕ_{rf}. Fig. 7 illustrates the effect of varying ϕ_{rf} on the resonance shape. Here we see experimentally how the sidebands change shape as the value of $\Delta\phi$ is changed. When $\Delta\phi$ is allowed to be a free parameter a good agreement is seen between the experimental data and the fit. All three fits yield consistent values for $\rho_{-,o}$ = 0.91(2) mm and $\rho_{+,o}$ = 0.11(1) mm. For each resonance ϕ_{rf} was incremented by 100°. Within 20% this phase dependence was reproduced in the fit parameter $\Delta\phi$.

As discussed earlier, only the third and fourth terms of Eq. 6 contain a $\Delta\phi$ term and contain the product of $\rho_{+,o}$ and $\rho_{-,o}$. While $\rho_{-,o}$ is introduced deliberately, a finite $\rho_{+,o}$ must be the result of an asymmetric injection of ions into the magnetic field of the Penning trap which leads to a pickup of cyclotron motion. If the amount of radial energy gained during the injection process can be reduced, then $\rho_{+,o}$ will be reduced, thus reducing the phase-dependent effect. This could be useful in fine-tuning the injection of ions into a Penning trap.

4 Octupolar Excitation

Excitation of ion motion in a Penning trap by application of an octupolar RF field at frequencies near $2\nu_c$ have been studied experimentally and in simulation. Single-ion simulations are used to explore the resonant response of ρ_+^2 for a variety of initial conditions. Simulations utilizing realistic distributions of multiple ions are used to predict resonance profiles under realistic conditions.

Experimental results together with those from simulation are used to make estimates of the initial ion cloud distribution.

4.1 Equations of motion

Calculating the electric field produced by a time-varying octupolar field produced by a set of electrodes at a radius a from the trap center yields the following field components:

$$\begin{aligned} E_x &= \ \ \tfrac{U_{rf}}{a^4}\sin(\omega_{rf}t+\phi_{rf})(y^3-3x^2y) \\ E_y &= -\tfrac{U_{rf}}{a^4}\sin(\omega_{rf}t+\phi_{rf})(x^3-3xy^2). \end{aligned} \tag{7}$$

Writing out the full equations of motion of an ion in a Penning trap subjected to an octupolar RF field using the transformation given in Eq. 2 yields

$$\begin{aligned} \dot{V}_x^{\pm} &= -\omega_{\pm}V_y^{\pm} - k\tfrac{(V_x^+-V_x^-)^2[(V_x^+-V_x^-)^2-3(V_y^+-V_y^-)^2]}{(\omega_+-\omega_-)^3} \\ \dot{V}_y^{\pm} &= \ \ \omega_{\pm}V_x^{\pm} + k\tfrac{(V_y^+-V_y^-)^2[(V_y^+-V_y^-)^2-3(V_x^+-V_x^-)^2]}{(\omega_+-\omega_-)^3} \end{aligned} \tag{8}$$

where

$$k = \frac{U_{rf}}{a^4}\frac{q}{m}\sin(\omega_{rf}t+\phi_{rf}). \tag{9}$$

Unfortunately, the transformation does not decouple the equations of motion. The ansatz presented in [12], $\overrightarrow{V}^{\pm} = \overrightarrow{A}^{\pm}(\mathrm{t})\mathrm{e}^{\pm i(\omega_{\pm}+\phi_{\pm})}$, where $A^{\pm}$ is an amplitude, does not simplify the problem. In the case of the quadrupolar excitation after the ansatz is inserted the high-frequency components can be neglected and the solution remains a physical description of the system. Following the

same procedure in the case of the octupolar excitation yields a non-physical description of the system. Unless a suitable coordinate transformation is found an analytical solution may not be possible. Numerical solutions to the equations of motion have to be used. By calculating the vectors $\overrightarrow{V}^{\pm}$ and using Eq. 1 it is possible to extract ρ_+ and ρ_- as a function of time. Since $E_r \propto \rho_+^2$, the radial energy pickup due to the application of an octupolar RF field is directly accessible.

4.2 Single-ion octupolar simulations

Octupolar excitation of the motion of a single ion will be used to illustrate the similarities and differences between the octupolar and quadrupolar excitation schemes.

4.2.1 Motional beating of single ions with $\nu_{RF} = 2\nu_c$

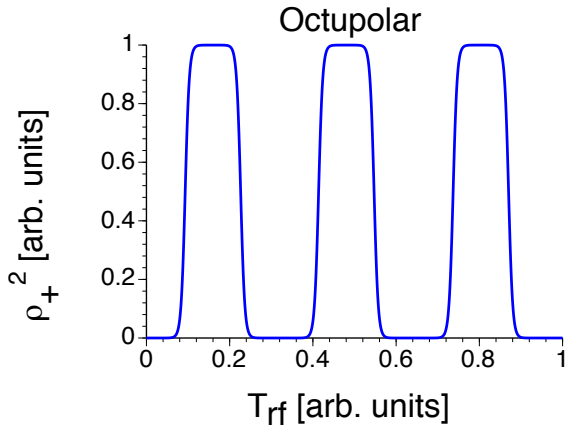

Fig. 8. ρ_+^2 of an ion confined in a Penning trap and subjected to an azimuthal octupolar RF field at frequency $2\nu_c$.

Fig. 8 plots ρ_+^2 of an ion as a function of time subjected to an azimuthal octupolar RF field. The ion is initially in a state of pure magnetron motion. A

periodic beat pattern is observed. Compared to the quadrupolar case (Fig. 5c) the beating is no longer harmonic but begins to approach a square wave in shape.

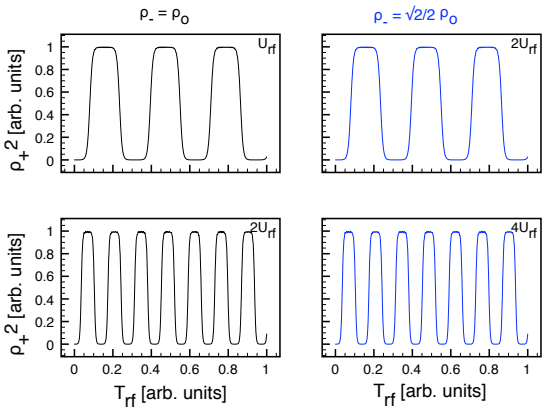

Fig. 9. The left hand plots show ρ_+^2 as a function of T_{rf} for an ion with an initial $\rho_{-,o} = \rho_o$ and $\rho_{+,o} = 0$ with applied RF amplitudes of U_{rf} and $2U_{rf}$, respectively. The right hand plots ρ_+^2 for an ion with an initial $\rho_{-,o} = \frac{\sqrt{2}}{2}\rho_o$ and applied RF amplitudes of $2U_{rf}$ and $4U_{rf}$, respectively.

According to Eq. 4, the beat frequency of an ion induced by a quadrupolar RF field with $\nu_{rf} = \nu_c$ is proportional to U_{rf}, and independent of the initial ion motion. This is not the case with the octupolar excitation. Fig. 9 displays the ρ_+^2 of a single ion, subjected to an octupolar field with $\nu_{rf} = 2\nu_c$, for different initial magnetron radii, $\rho_{-,o}$, and applied RF amplitudes, U_{rf}. The plots on the left hand display the beat patterns for an ion with an initial magnetron radius of ρ_o. Doubling U_{rf} results in an increase in the beat frequency. The plots on the right illustrate that doubling U_{rf} and scaling the initial magnetron radius by $\sqrt{2}/2$ preserves the original beat frequency. In the case of octupolar excitation the beat frequency depends not only on the excitation amplitude, but also on the initial motion of the ion in the trap.

Fig. 10 plots the beat frequency as a function of the initial $\rho_{-,o}$ for three

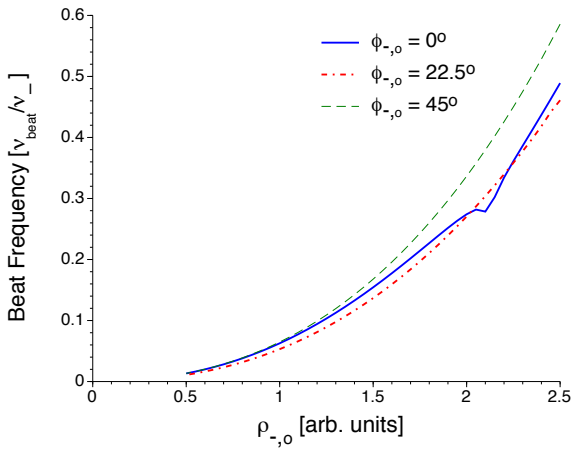

Fig. 10. Beat frequency between magnetron and cyclotron motions as a function of $\rho_{-,o}$ for constant U_{rf} and for three initial magnetron phases, $\phi_{-,o} = 0°, 22.5°$ and 45°.

different initial magnetron phases, $\phi_{-,o}$. The figure reveals that the beat frequency depends not only on $\rho_{-,o}$, but also on $\phi_{-,o}$. The dip in the $\phi_{-,o} = 0°$ curve is not a numerical artifact, but has been verified by two independent simulations. By changing the phase one can change the position of this dip, but quickly moves to a larger value of $\rho_{-,o}$ as one moves away from $\phi_{-,o} = 0°$. With $\phi_{rf} = 0°$ the dip occurs at $\rho_- \sim 2.1$ and $\nu_{beat}/\nu_- \sim 0.26$. Fig. 9 might lead one to believe that $\nu_{beat} \propto \rho^2_{-,o} \cdot U_{rf}$, yet taking Fig. 10 into account the relation would need to be amended to $\nu_{beat} \propto f(\phi_-) \cdot \rho^2_{-,o} \cdot U_{rf}$. Holding U_{rf} and $\phi_{-,o}$ constant and plotting the beat frequency as a function of $\phi_{-,o}$ yields Fig. 11. The beat frequency seems to sample the octupolar RF field's spatial orientation, and is at a minimum at the anti-nodes, and maximum at the nodes, of the field.

According to Eq. 4 the beat frequency in the case of $\nu_{rf} = \nu_c$ due to a quadrupolar excitaton is linear with respect to U_{rf} and is phase independent. Again, this is different in the case of octupolar excitation. The beat frequency is not linear with respect to U_{rf}, and is dependent upon the $\phi_{-,o}$,

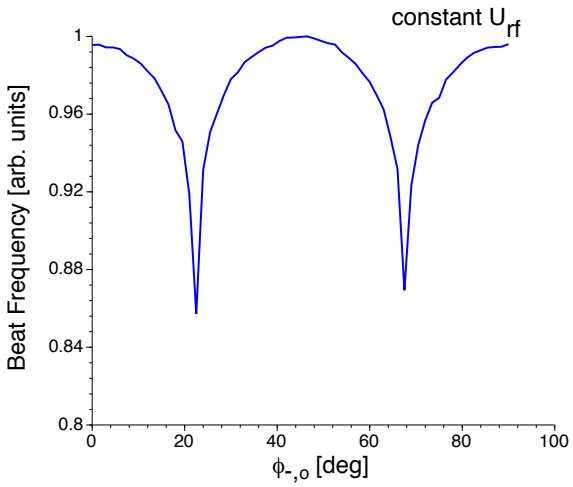

Fig. 11. Beat frequency as a function of $\phi_{-,o}$ for a constant U_{rf}.

as is illustrated in Fig. 12 which plots the beat frequency as a function of U_{rf}. As the beat frequency nears ν_- the beat frequency begins to lose its periodic nature. Zooming in to low frequencies and excitation amplitudes the $\phi_{-,o} = 0°$ and $\phi_{-,o} = 45°$ curves become indistinguishable, while the $\phi_{-,o} = 22.5°$ curve deviates. Again, similar to Fig. 10, a dip is observed in the $\phi_{-,o} = 0°$ case, again located at $\nu_{beat}/\nu_- \sim 0.26$.

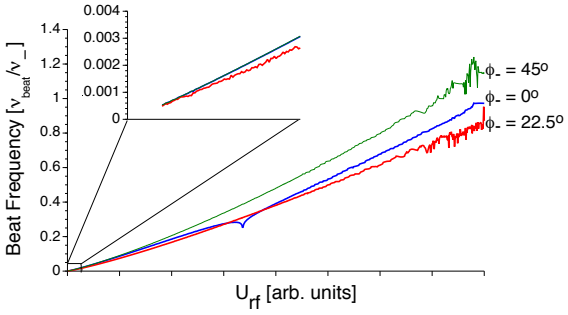

Fig. 12. Beat frequency as a function of U_{rf} for three initial $\phi_{-,o}$'s. The insert zooms in to low beating frequencies and amplitudes.

We are now in a position to investigate a possible invariant of the motion. Fig. 13 shows the beat frequency when changing $\rho_{-,o}$, while at the same time keeping the product $U_{rf} \cdot \rho^2_{-,o}$ constant. It can be seen that the beat frequency is constant for a given initial phase, $\phi_{-,o}$. This was found to be not only true

for ions in a state of pure magnetron motion, but for mixed initial motions, $\rho_o = \sqrt{\rho_{+,o}^2 + \rho_{-,o}^2}$, as well. Therefore, we arrive at a general relationship $\nu_{beat} \propto \alpha(\rho_{\pm,o}, \phi_{\pm,o}, \phi_{rf}) \cdot \rho_o^2 \cdot U_{rf}$, where α is a scaling factor which depends on all four of the initial ρ's and ϕ's.

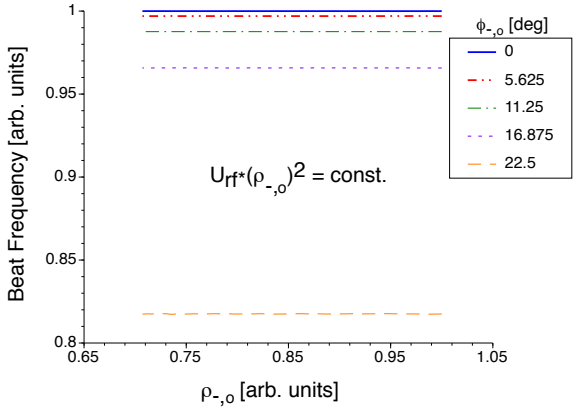

Fig. 13. Beat frequency due to an octupolar excitation as a function of $\rho_{-,o}$ holding $\rho_{-,o}^2 \cdot U_{rf}$ constant for several values of $\phi_{-,o}$.

4.2.2 Invariant phase relation of the octupolar excitation

According to Eq. 5, $\Delta\phi = \phi_{rf} - (\phi_+ + \phi_-)$ is a constant of the motion for a quadrupolar excitation. We investigate if a similar phase relation holds for the octupolar excitation.

Fig. 14 shows scans of ρ_+^2 as a function of $\phi_{+,o}$ and time for a given $\phi_{-,o}$ with $\phi_{rf} = 0°$ in all cases. By comparing the patterns it is easy to conclude that the time dependence of ρ_+^2 is the same if $\phi_{+,o} + \phi_{-,o} = \text{const}$. It was verified that this also holds true if ϕ_{rf} is changed.

Fig. 15 is similar to Fig. 14, except $\phi_{+,o}$ is held constant at 0° and the individual plots are ρ_+^2 as a function of $\phi_{-,o}$ and time. Here we verified that for $\phi_{+,o} = 0°$, $\frac{1}{2}\phi_{rf}$ - $\phi_{-,o} = \text{const}$. the same time dependence of ρ_+^2 is observed. Testing

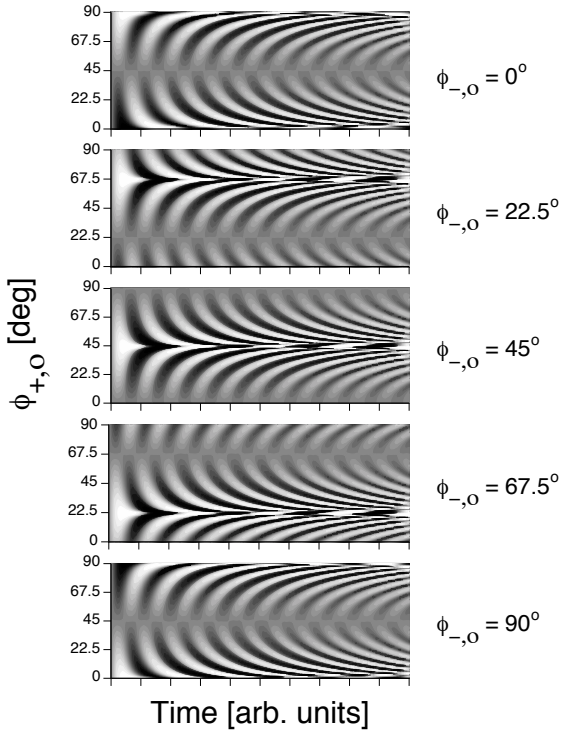

Fig. 14. 2D simulations of ρ_+^2 as a function of time and $\phi_{+,o}$ for a given $\phi_{-,o}$ with $\phi_{rf} = 0°$. The grey scale is proportional to ρ_+^2.

this condition for many values of $\phi_{+,o}$ yields the same results and leads us to conclude that the invariant phase in the case of octupolar excitation is $\Delta\phi = \frac{1}{2}\phi_{rf}$ - $(\phi_+ + \phi_-)$. This differs from the quadrupolar phase relation, Eq. 5, only in the factor of 1/2 multiplying the ϕ_{rf} term. This appears plausible as the octupolar field has twice the number of nodes and anti-nodes as the quadrupolar field. The factor of 1/2 reflects that the ions begin their motion at the same position with respect to the field orientation.

4.2.3 Single-ion resonance curves

To begin, we will examine octupolar resonances of single ions initially in a state where $\rho_o = \rho_{-,o}$. The general observation is a periodic change of ρ_+^2 as a function of U_{rf}. Along the line $\nu_{rf} = 2\nu_c$ a resonant effect is observed. Fig. 16

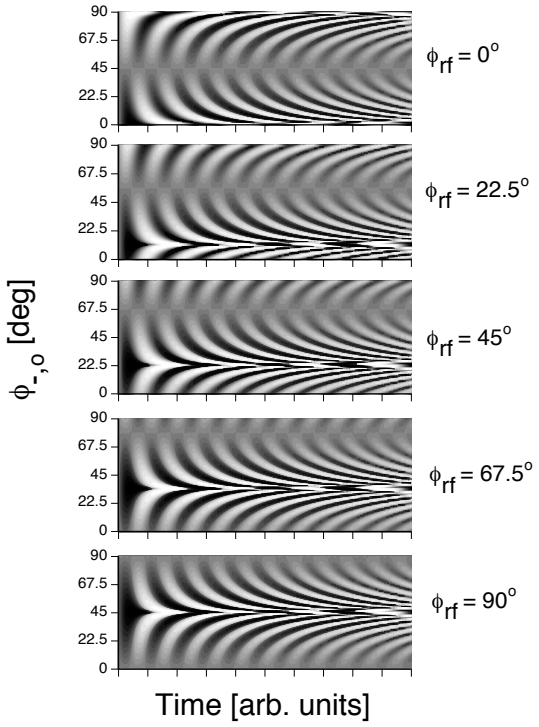

Fig. 15. 2D simulations of ρ_+^2 as a function of time and $\phi_{-,o}$ for a given ϕ_{rf} with $\phi_{+,o} = 0°$. The grey scale is proportional to ρ_+^2.

illustrates the dependence of ρ_+^2 on frequency detuning, $\Delta\nu = \nu_{rf}$ - $2\nu_c$, and U_{rf} for various values of $\phi_{-,o}$. At $\phi_{-,o} = 13.5°$ a secondary resonant effect becomes visible which sweeps through the primary resonant structure as the value of $\phi_{-,o}$ is changed. This effect is on a line with an origin at $U_{rf} = 0$ and $\Delta\nu = 0$ which rotates clockwise for increasing values of $\phi_{-,o}$. At $\phi_{-,o} = 18.0°$ the structure can be seen across all three sections of the primary resonant structure. At $\phi_{-,o} = 22.5°$ the secondary structure lies on the $\Delta\nu = 0$ line.

Looking closely at the resonances reveals a narrowing of the resonance profiles at $\Delta\nu = 0$ for certain values of U_{rf}. Fig. 17 plots 2D cuts from the $\phi_{-,o} = 0°$ (left) and $\phi_{-,o} = 22.5°$ (right) cases shown in Fig. 16. Moving from the top plots to the bottom steps through the first conversion of magnetron to cyclotron motion. The $\phi_{-,o} = 0°$ case exhibits a larger width in the radial

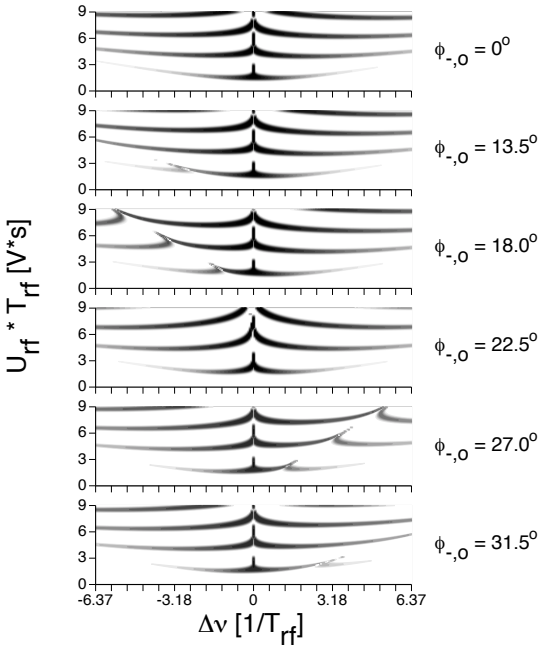

Fig. 16. Simulation of ρ_+^2 for a single ion with $\rho_{-,o} = 1$ mm and $\rho_{+,o} = 0$ mm as a function of frequency detuning, $\Delta\nu = \nu_{rf}$ - $2\nu_c$, and U_{rf} for different values of $\phi_{-,o}$. The grey scale is proportional to ρ_+^2.

energy distribution at the lower values of $U_{rf}{\cdot}T_{rf}$ as in $\phi_{-,o} = 22.5°$ case. The central peak narrows for larger values of $U_{rf}{\cdot}T_{rf}$ and at $U_{rf}{\cdot}T_{rf} = 2.90$ V·s the radial energy gained during the excitation begins to drop. The top three plots of the $\phi_{-,o} = 22.5°$ case show a suppression of radial energy at $\Delta\nu \approx 2\nu_c$. The bottom three plots no longer exhibit this behavior, but the central peak continues to narrow. In both cases $\Delta\nu_{FWHM}$ falls below $1/(100{\cdot}T_{rf})$, which corresponds to a factor of ~ 200 increase in resolving power over the quadrupolar excitation for the same excitation time! It remains to be seen how well the ions can be prepared to reproduce these results under realistic conditions.

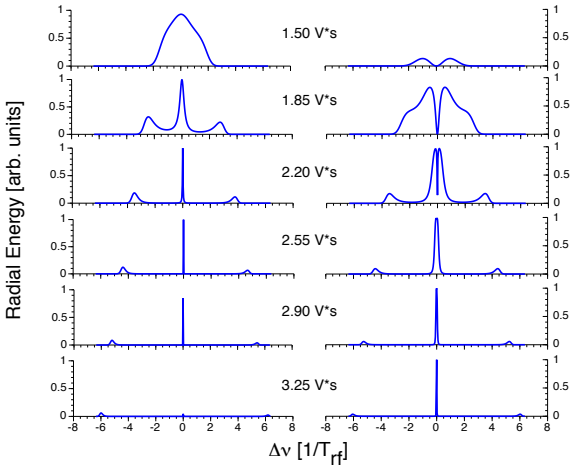

Fig. 17. 2D cuts from the $\phi_{-,o}- = 0°$ and $\phi_{o,-}- = 22.5°$ 3D profiles in Fig. 16 for six different values of $U_{rf} \cdot T_{rf}$.

4.2.4 Realistic multi-ion simulations

Simulations involving multiple ions representing a cloud are required to study the ion behavior in the case of an octupolar excitation under realistic conditions. First we will examine the radial energy gain as a function of U_{rf}, with $\nu_{rf} = 2\nu_c$. Gaussian distributions were used in generating values for the initial ion cloud. Fig. 18 shows the results of three simulations for three different values of $\sigma_{\rho_{-,o}}$ with $\overline{\rho}_{-,o} = 0.55$ mm. $\rho_{+,o} = 0.050(5)$ mm was used, being a conservative estimate from simulated radial energy gain during injection into the Penning trap. This value also agrees with those obtained from fits to quadrupolar resonances obtained under similar conditions. Widths of the ϕ distributions seem to have a small effect on the multi-ion response curves, and $\phi_- = 0(5)°$ and $\phi_+ = 0(50)°$ were used. For the largest value of $\sigma_{\rho_{-,o}}$ shown in Fig. 18 the curve seems to mimic the behavior of a damped oscillator, converging to some average asymptotical value of radial energy. This is the result of the beat frequency being dependent on ρ_o, as discussed in Sec. 4.2.1. The larger the spread in ρ_o, the larger the range of beat frequencies. The distri-

bution of beat frequencies determines how quickly the average beat pattern is damped.

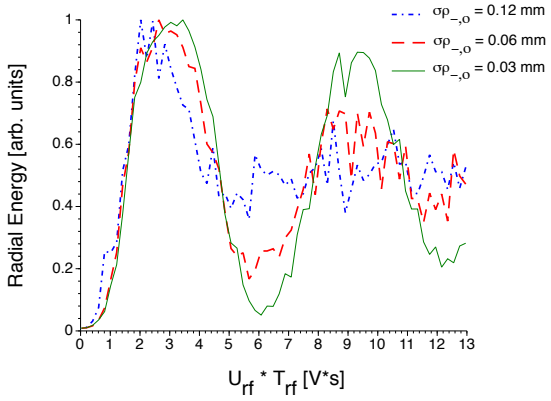

Fig. 18. Simulated radial energy gain for three different values of $\sigma_{\rho_{-,o}}$ as a function of U_{rf} for $\nu_{rf} = 2\nu_c$ and $\overline{\rho}_- = 0.55$ mm.

Fig. 19 plots the results from two octupolar simulations of $^{23}Na^+$ with $T_{rf} =$ 50 ms. Both simulations were performed with identical phase and ρ_+ distributions as the simulations shown in Fig. 18. $\overline{\rho}_-$ was also held constant, but the widths of the distributions were changed. The simulation in the first column was performed with $\rho_{-,o} = 0.8000(325)$ mm and the the second with $\rho_{-,o} =$ 0.80(13) mm. Instead of ρ_+^2 the calculated time of flight was plotted for easier comparison to experimental results covered in the next chapter. The plots in the first row show the dependence of the time of flight as a function of U_{rf} and $\Delta\nu$. The grey scale indicates smaller values of time of flight. The plots in the remaining rows are cuts at different voltages.

Note the resemblance of the top left plot to the single-ion case shown in Fig. 16. For the larger $\sigma_{\rho_{-,o}}$, shown on the right, only one conversion is seen in the grey-scale plot before settling down to an average value. This is also reflected in Fig. 18. The 2D profiles also reveal that there is a greater separation in time of flight between the baseline and the minimum for the profiles on the

left. In both cases as one proceeds from smaller to larger values of U_{rf} the resonance narrows. On the right-hand side the narrow peak begins to develop on top of a broader resonant structure, while on the left the time of flight baseline doesn't change. At $U_{rf} = 44.5$ V the resonance curve on the left has achieved a maximum change in time of flight and a minimal width of $\sim 0.14/T_{rf}$, corresponding to a gain of a factor of 13 in resolving power over the quadrupolar excitation.

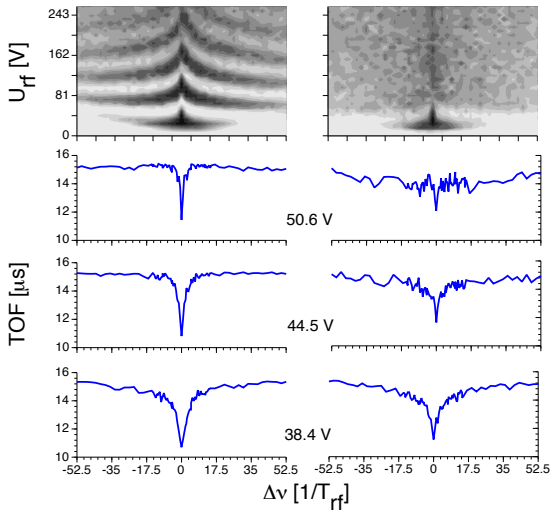

Fig. 19. (Left): multi-ion simulation of TOF as a function of U_{rf} and $\Delta\nu$ with three cuts at different RF voltages. (Right): same as the left only the width of the $\rho_{-,o}$ distribution has been increased by a factor of 4.

4.3 Experimental procedure and results

Fig. 20 presents a schematic drawing of the electronic setup which was used to produce an azimuthal octupolar RF field in the LEBIT Penning trap. An arbitrary function generator (AFG) prodives a signal to a broadband RF amplifier with 65 dB gain. The signal from the amplifier is fed into a phase-splitting coil. The two output signals, $U_{rf,1}$ and $U_{rf,2}$, which are 180° out of phase, are

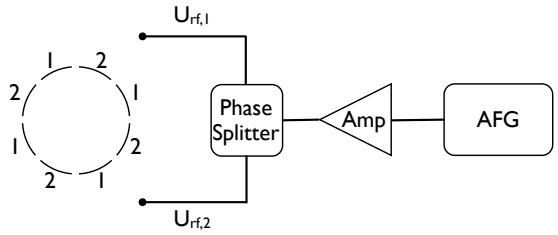

Fig. 20. Schematic drawing of experimental setup used to produce a azimuthal octupolar RF field in the LEBIT Penning trap.

then fed into the ring electrode segments. The amplitudes of the two phases agree to within $\sim$ 15-20 %. From now on, their average will be quoted as the excitation amplitude, U_{rf}.

In the experiments $^{23}Na^{+}$ ions were used. Ion bunches from the cooler/buncher were injected off-axis, via the Lorentz steerer, mentioned above, and trapped in the LEBIT high-precision Penning trap.

4.3.1 Experimental octupolar studies in resonance

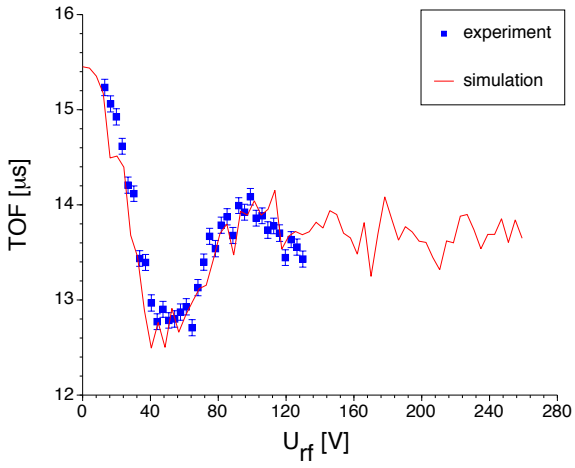

Fig. 21. Time of flight as a function of U_{rf} for a octupolar excitation of $^{23}Na^{+}$ with T_{rf} = 50 ms at $\nu_{rf} = 2\nu_c$. The solid line shows a simulation.

$^{23}Na^{+}$ ions were excited with an octupolar excitation with $\nu_{rf} = 2\nu_c$ for T_{rf}

= 50 ms and their time of flight was measured as a function of U_{rf}. The result is shown in Fig. 21 together with a simulated curve. The simulated curve corresponds to the $\sigma_{\rho_{-,o}} = 0.13$ mm case from Fig. 18. In order to get a good agreement between experimental data and the simulation results it was necessary to divide RF voltage values measured at the output of the circuit by a factor of 0.7. Such a factor makes sense as it accounts for RF attenuation and partial shielding due to the geometry of the trap. Using experimental data like that shown in Fig. 21 and comparing to the corresponding simulation results allows the values of $\overline{\rho}_{-,o}$ and $\sigma_{\rho_{-,o}}$ to be determined. The minimum time-of-flight value achieved is a function, primarily, of $\overline{\rho}_{-,o}$, and the damping of the curve is determined by the ratio of $\sigma_{\rho_{-,o}}$ and $\overline{\rho}_{-,o}$.

In the case of quadrupolar excitation, the beat frequency of $\rho_+^2(t)$ is proportional to the product $U_{rf} \cdot T_{rf}$ (see Eq. 4). We will experimentally explore if this holds true for the octupolar excitation, as well. Fig. 22 plots time of flight of ions as a function of U_{rf} for five different excitation times. As expected, the minimum time of flight is reached at a lower value of U_{rf} for longer excitation times. The value of U_{rf} where the TOF curve reaches its minimum will be labeled U_o. Fig. 23 displays the product $U_o \cdot T_{rf}$ for the fives cases shown in Fig. 22, along with simulated data using our best-fit parameters determined by the comparison shown in Fig. 21. Both the experimental and simulated data agree and are constant within 5%. This value will not be constant for all circumstances, and depends on initial conditions.

By adjusting the Lorentz steerer we can control $\overline{\rho}_{-,o}$. The displacement of the ions as a function of the applied voltage is linear. Fig. 24 shows six different octupolar scans of TOF as function of U_{rf} in the case of $\nu_{rf} = 2\nu_c$ for six different voltages,V_L, applied to the Lorentz steerer. The first minimum in

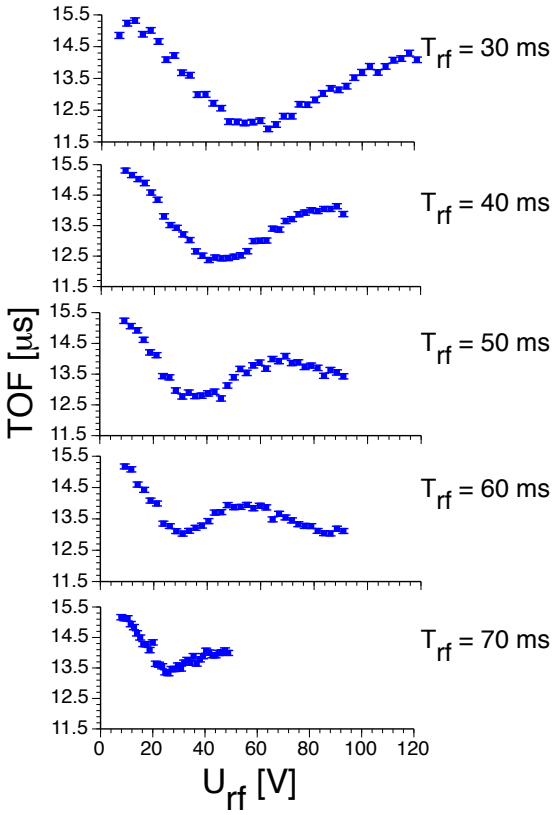

Fig. 22. Octupolar TOF curves of $^{23}Na^{+}$ as a function of U_{rf} with $\nu_{rf} = 2\nu_c$ for several excitation times.

the curves represent the necessary U_{rf} to, on average, bring the ions to a state of maximum radial energy.

Fig. 25 plots the beat frequencies observed in Fig. 24 as a function of $\rho_{-,o}$. Two of the curves are simulation results and one is experimental data. The experimental observation does not seem to confirm the nonlinear response illustrated in Fig. 10. However, the $\sigma_{\rho_{-,o}} = 0.13$ mm curve represents our best-fit simulation scenario, and matches the data quite well. The third curve reduces the best-fit value of $\sigma_{\rho_{-,o}}$ by a factor of four to 0.0325 mm. Now the curve begins to recover the nonlinear shape shown in the single ion simulations. Again the variation of individual beating frequencies of ions in the cloud play a dominant role in determining the overall response of the system.

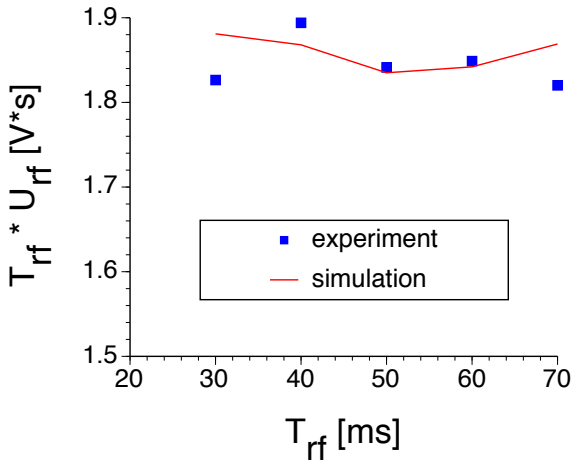

Fig. 23. Product of U_o and T_{rf}, where T_{rf} is the duration of the octupolar excitation and U_o is the amplitude of applied octupolar RF field at which the TOF curve reaches its minimum.

4.3.2 Experimental octupolar resonances

Fig. 26 displays several octupolar resonances of $^{23}Na^+$ produced with $T_{rf} = 50$ ms for various values of U_{rf}. Included in the figures are simulated resonances which were produced using the same initial conditions as the simulation in the right column of Fig. 19. For $U_{rf} \leq 40$ V the width of the resonances are between $1.3/T_{rf}$ and $0.9/T_{rf}$. Proceeding towards larger amplitudes reduces this width. At $U_{rf} = 72.9$ V a narrow resonant peak with a width of $\sim 0.2/T_{rf}$ forms atop a broader resonant structure.

4.3.3 Mass measurements with octupolar excitation

To verify that octupolar resonances can be used for precision mass measurements, a mass measurement of $^{41}K^+$, using $^{39}K^+$ as a reference, was performed. An excitation time of $T_{rf} = 200$ ms was used in each individual measurement. U_{rf} was chosen such that the resonances were Gaussian, resembling the resonance shown in Fig. 4. Fig. 27 shows the results of this mass measurement. As

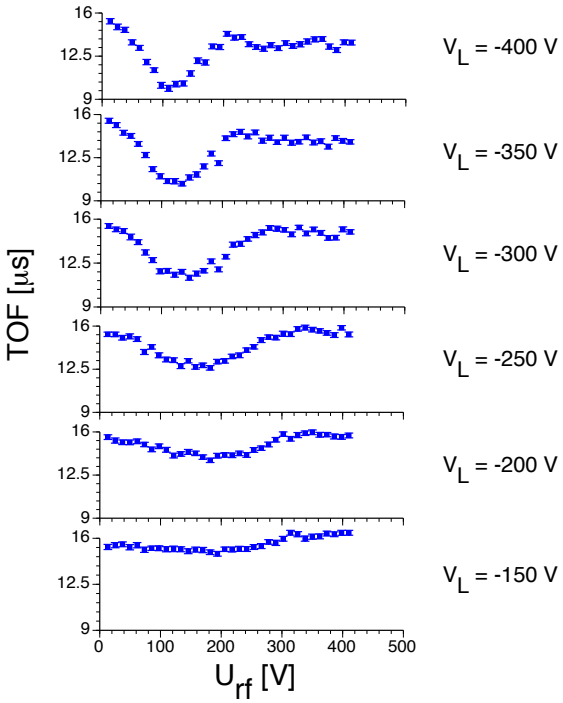

Fig. 24. Time of flight as a function of U_{rf} with $\Delta\nu = 0$ using $^{23}Na^{+}$ with $T_{rf} = 50$ ms octupolar excitation for six different Lorentz steerer voltages, V_L. The greater the magnitude of applied voltage, the larger the initial average displacement of the ions from the center of the trap.

there is no theoretical line shape all resonances were fit with a Gaussian profile. What is plotted is the difference of the mean mass value extracted from the octupolar measurements from the accepted literature values (Atomic Mass Evaluation [22]). The dashed lines represent the uncertainty in the mean of the experimental results. The solid lines represent the uncertainty in the AME values. As can be seen, there is excellent agreement within the uncertainty.

5 Summary and Conclusions

Although an analytical solution to the octupolar excitation has yet to be found, numerical simulations combined with experimental results have offered

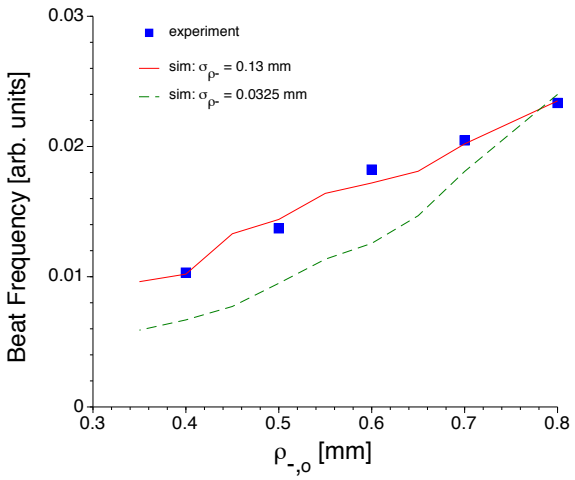

Fig. 25. Beat frequency as a function of $\overline{\rho}_{-,o}$. The experimental curve is extracted from data shown in Fig. 24. The $\sigma_{\rho_{-,o}} = 0.13$ mm curve is a simulation based on the parameters extracted from the simulation shown in Fig. 21. The second simulated curve was generated using identical parameters, except $\sigma_{\rho_{-,o}} = 0.0325$ mm.

significant insight into this complicated problem. The most important observations can be summarized as:

- *The beat frequency of an ion subjected to an octupolar RF excitation applied at $\nu_{RF} = 2\nu_+ + 2\nu_- = 2\nu_c$ is dependent upon the initial conditions of the ion motion. This is in contrast to the quadrupolar excitation at ν_c where such a dependence does not exist.*
- *The octupolar resonance profiles have a radically different shape than their quadrupolar counterparts.*
- *For certain initial conditions it is possible to reduce the width of octupolar resonances by a factor of 10 or more beyond what is achievable with a comparable quadrupolar resonance performed with the same excitation time.*

We have verified a factor 5 gain in resolving power over the standard quadrupolar excitation scheme. We have also shown that the initial conditions of the

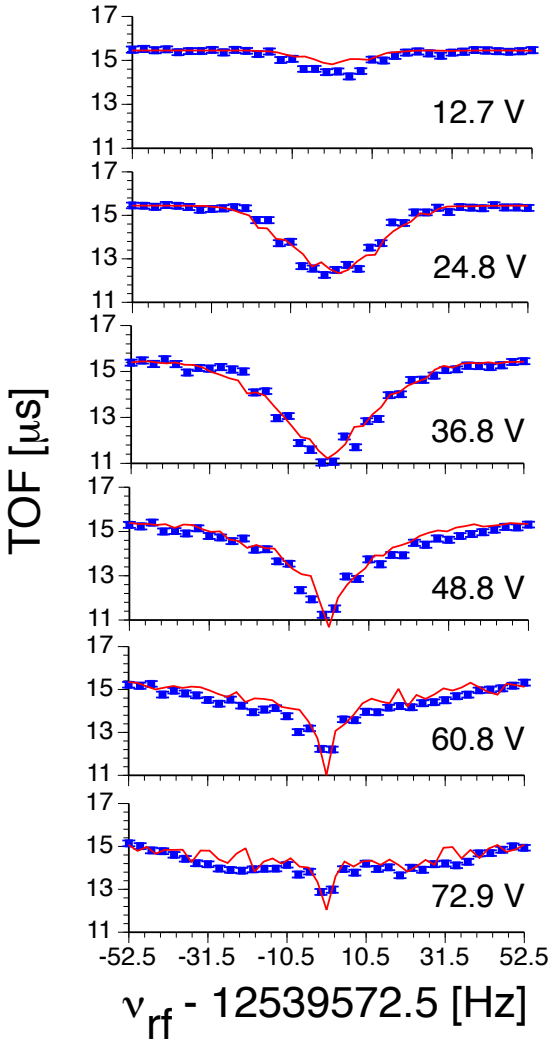

Fig. 26. Several octupolar resonance profiles of $^{23}Na^{+}$ with T_{rf} = 50 ms for various values of U_{rf} (data points) compared with simulated results (solid lines).

ion cloud determines the ultimate resolving power that can be achieved. Simulations show even higher resolving powers are possible, provided that the ions can be prepared appropriately. Although more work is required to assess the absolute accuracy of mass measurements performed with octupolar excitations, a promising first step has been taken towards the implementation of octupolar resonances in high-precision mass measurements. Motivated by the phase dependence exhibited by the octupolar excitation, we have also revisited the quadrupolar excitation and confirmed a phase dependence of

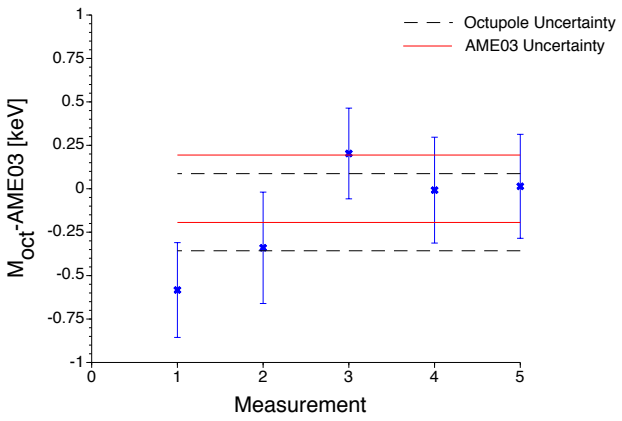

Fig. 27. Mass comparison of $^{39,41}K^{+}$ using octupolar excitation. $^{39}K^{+}$ was used as the reference and all measurements were performed with 200 ms excitation times. resonance line shapes.

References

[1] M. Bradley, J. Porto, S. Rainville, J. Thompson, D. Pritchard, Phys. Rev. Lett. 83 (1999) 4519.

[2] W. Shi, M. Redshaw, E. Meyers, Phys. Rev. A 72 (2005) 022510.

[3] I. Berström, C. Carlberg, T. Fritioff, G. Douysset, J. Schonfelder, R. Schuch, Nucl. Instrum. Methods A 487 (2002) 618.

[4] G. Bollen, D. Davies, M. Facina, J. Huikari, E. Kwan, P. A. Lofy, D. J. Morrissey, A. Prinke, R. Ringle, J. Savory, P. Schury, S. Schwarz, C. Sumithrarachchi, T. Sun, L. Weissman, Phys. Rev. Lett. 96 (2006) 152501.

[5] A. Kellerbauer, G. Audi, D. Beck, K. Blaum, G. Bollen, B. A. Brown, P. Delahaye, C. Guénaut, F. Herfurth, H.-J. Kluge, D. Lunney, S. Schwarz, L. Schweikhard, C. Yazidjian, Phys. Rev. Lett. 93 (2004) 072502.

[6] G. Bollen, S. Becker, H.-J. Kluge, M. König, R. Moore, T. Otto, H. Raimbault-Hartmann, G. Savard, L. Schweikhard, H. Stolzenberg, Nucl. Instrum. Methods

A 368 (1996) 675.

[7] R. Ringle, P. Schury, T. Sun, G. Bollen, D. Davies, J. Huikari, E. Kwan, D. Morrissey, A. Prinke, J. Savory, S. Schwarz, C. Sumithrarachchi, Int. J. Mass Spec. Ion. Proc. 251 (2-3) (2006) 300.

[8] P. Schury, G. Bollen, D. Davies, A. Doemer, D. Lawton, D. Morrissey, J. Ottarson, A. Prinke, R. Ringle, T. Sun, S. Schwarz, L. Weissman, Eur. Phys. J. A 25(S1) (2005) 51.

[9] G. Sikler, D. Ackermann, G. Bollen, F. Attallah, D. Beck, J. Dilling, S. A. Elisseev, H. Geissel, D. Habs, S. Heinz, F. Herfurth, Nucl. Instr. and Meth. B 204 (2002) 482.

[10] G. Savard, R. C. Barber, D. Beeching, F. Buchinger, J. E. Crawford, S. Gulick, X. Feng, E. Hagberg, J. Hardy, V. T. Koslowsky, J. K. P. Lee, R. Moore, K. S. Sharma, M. Watson, Nucl. Phys. A 368 (1997) 353.

[11] V. S. Kolhinen, T. Eronen, J. Hakala, A. Jokinen, S. Kopecky, S. Rinta-Antila, J. Szerypo, J. Äystö, Nucl. Instrum and Methods in Phys. Res. B 204 (2003) 502.

[12] M. König, G. Bollen, H.-J. Kluge, T. Otto, J. Szerypo, Int. J. Mass Spec. Ion. Proc. 142 (1995) 95.

[13] G. Gräff, H. Kalinowsky, J. Traut, Z. Phys. A297 (1980) 35.

[14] J. Dilling, R. Baartman, P. Bricault, M. Brodeur, L. Blomeley, F. Buchinger, J. Crawford, J. Crespo López-Urrutia, P. Delheij, M. Froese, G. Gwinner, Z. Ke, J. K. P. Lee, R. Moore, V. Ryjkov, G. Sikler, M. Smith, J. Ullrich, J. Vaz, T. Collaboration, Int. J. Mass Spec. 251 (2006) 198.

[15] S. Schwarz, G. Bollen, D. Lawton, P. Lofy, D. J. Morrissey, J. Ottarson, R. Ringle, P. Schury, T. Sun, V. Varentsov, L. Weissman, Nucl. Instr. and Meth. B 204 (2003) 507.

[16] S. Eliseev, M. Block, A. Chaudhuri, F. Herfurth, H.-J. Kluge, A. Martin, C. Rauth, G. Vorobjev, this volume.

[17] G. Bollen, S. Schwarz, D. Davies, P. Lofy, D. Morrissey, R. Ringle, P. Schury, T. Sun, L. Weissman, Nucl. Instr. and Meth. A 532 (2004) 203.

[18] T. Sun, S. Schwarz, G. Bollen, D. Lawton, R. Ringle, P. Schury, Eur. Phys. J. A 25(S1) (2005) 61.

[19] G. Bollen, R. Moore, G. Savard, H. Stolzenberg, J. Appl. Phys. 68 (1990) 4355.

[20] G. Bollen, H.-J. Kluge, T. Otto, G. Savard, L. Schweikhard, H. Stolzenberg, G. Audi, R. Moore, G. Rouleau, J. Mod. Optics 39 (1992) 257.

[21] L. Brown, G. Gabrielse, Rev. Mod. Phys. 58 (1986) 233.

[22] G. Audi, A. H. Wapstra, C. Thibault, Nucl. Phys. A 729 (2003) 337.